

# An Eulerian approach to the simulation of deformable solids: Application to finite-strain elasticity

Ken Kamrin<sup>a,\*</sup>, Jean-Christophe Nave<sup>b</sup>

<sup>a</sup>*School of Engineering and Applied Sciences, Harvard University Cambridge, MA 01238, USA*

<sup>b</sup>*Department of Mathematics, Massachusetts Institute of Technology, Cambridge, MA 02139, USA*

---

## Abstract

We develop a computational method based on an Eulerian field called the “reference map”, which relates the current location of a material point to its initial. The reference map can be discretized to permit finite-difference simulation of large solid-like deformations, in any dimension, of the type that might otherwise require the finite element method. The generality of the method stems from its ability to easily compute kinematic quantities essential to solid mechanics, that are elusive outside of Lagrangian frame. This introductory work focuses on large-strain, hyperelastic materials. After a brief review of hyperelasticity, a discretization of the method is presented and some non-trivial elastic deformations are simulated, both static and dynamic. The method’s accuracy is directly verified against known analytical solutions.

---

## 1. Introduction

Two perspectives are used for modeling solid and amorphous materials in the continuum limit. Physicists and rheologists tend to prefer an Eulerian treatment where the material can be viewed essentially as a fluid equipped with state variables that provide “memory” (see [4, 10]). On the other hand, many in the engineering community prefer a Lagrangian description, where the material body is decomposed as a network of volume elements that deform under stress (see [1, 5]).

Continuum mechanical laws derive from point-particle mechanics applied to a continuum element. The primitive form is resultantly Lagrangian, though an Eulerian conversion can always be asserted— one rewrites the constitutive laws in rate form and expands all material time derivatives in terms of fixed-space derivatives. Be that as it may, a rigorous Eulerian switch can be a painstaking mathematical task. This is especially true of solid-like constitutive laws, which often depend on nonlinear tensor operations and coupled history-dependent state variables, leading to unduly complicated Eulerian rate expansions [7].

To dodge these difficulties, those preferring Eulerian-frame have generally resorted to approximations or added conditions that simplify the final constitutive form. While sometimes warranted, the connection back to Lagrangian mechanics becomes clouded, complicating the process of deriving physically motivated constitutive behavior.

In this paper, a field we call the “reference map” is utilized to construct and implement solid-like constitutive laws in Eulerian-frame with *no* added approximations. The way the map provides “memory” to the system admits immediate computation of kinematic variables crucial to Lagrangian solid mechanics. To maintain a clear presentation, several avenues of motivation are first provided that discuss the necessary laws of continuum mechanics and the basic quantities of solid kinematics. The theory of large-strain elasticity, hyperelasticity, is then sketched. In particular, by enabling

---

\*Corresponding author.

*Email addresses:* [kkamrin@seas.harvard.edu](mailto:kkamrin@seas.harvard.edu) (Ken Kamrin), [jcnave@mit.edu](mailto:jcnave@mit.edu) (Jean-Christophe Nave)

*URL:* <http://people.seas.harvard.edu/~kkamrin/> (Ken Kamrin), <http://www.mit.edu/~jcnave/> (Jean-Christophe Nave)

quick access to the *deformation gradient* tensor, the reference map can be used to accurately compute solid deformations without the approximations, ambiguities, or pre-conditions of other Eulerian approaches. Three non-trivial deformations are then simulated to verify these points.

## 2. Basics

In Eulerian frame, the flow or deformation of a canonical continuous material can be calculated by solving a system of equations that includes:

$$\rho_t + \nabla \cdot (\rho \mathbf{v}) = 0 \quad (1)$$

$$\nabla \cdot \mathbf{T} + \rho \mathbf{g} = \rho(\mathbf{v}_t + \mathbf{v} \cdot \nabla \mathbf{v}) \quad (2)$$

$$\mathbf{T}^T = \mathbf{T}. \quad (3)$$

The first equation upholds mass conservation, and the next two, respectively, uphold conservation of linear and angular momentum. The flow is described by the velocity field  $\mathbf{v}(\mathbf{x}, t)$  and the stresses by the Cauchy stress tensor  $\mathbf{T}(\mathbf{x}, t)$ , which includes pressure contributions. A constitutive law is then asserted to close the system of equations.

## 3. Solid kinematics

We ultimately intend our approach to apply to any material with a “solid-like” constitutive law. By solid-like, we mean specifically laws that express the stress tensor in terms of some kinematic quantity that measures the local deformation from some nearest relaxed state. This trait reflects the microscopic basis of solid stress as arising from potential energy interactions between material microconstituents. The simplest solid-like response is isothermal elasticity, where total deflection under loading immediately determines the stresses within [5]. A less basic example would be elastoplasticity, where internal stresses derive from a small elastic component of the total strain. Here, the nearest relaxed state can differ from the original unstressed state and may depend on evolving state parameters, temperature, and/or rate [9].

To encompass the broad definition above, a continuum description for solid-like materials necessitates a rigorous way of tracking local relative displacements over some finite time period. Without making any “small displacement” approximations, a general and robust continuum framework calls for a kinematic field  $\chi$  known as the *motion function*. Suppose at time  $t = 0$ , that a body of material is in an unstressed *reference configuration*. The body then undergoes a deformation process such that at time  $t$ , an element of material originally at  $\mathbf{X}$  has been moved to  $\mathbf{x}$ . The motion is defined by  $\mathbf{x} = \chi(\mathbf{X}, t)$ . We say that the body at time  $t$  is in a *deformed configuration*.

The motion can be used to define the *deformation gradient*  $\mathbf{F}$ , which is of crucial importance in continuum solid mechanics:

$$\mathbf{F}(\mathbf{X}, t) = \frac{\partial \chi(\mathbf{X}, t)}{\partial \mathbf{X}} \quad \text{or} \quad F_{ij} = \frac{\partial \chi_i(\mathbf{X}, t)}{\partial X_j}. \quad (4)$$

Note that we use  $\nabla$  for gradients in  $\mathbf{x}$  only, and always write gradients in  $\mathbf{X}$  in derivative form as above. As per the chain rule, the  $\mathbf{F}$  tensor describes local deformation in the following sense: If  $d\mathbf{X}$  represents some oriented, small material filament in the reference body, then the deformation process stretches and rotates the filament to  $d\mathbf{x} = \mathbf{F} d\mathbf{X}$  in the deformed body. Also, the evolution of  $\mathbf{F}$  can be connected back to the velocity gradient via

$$\dot{\mathbf{F}} = (\nabla \mathbf{v}) \mathbf{F} \quad (5)$$

where we use  $\dot{\phantom{x}}$  for material time derivatives.

Since  $\det \mathbf{F} > 0$  for any physical deformation, the deformation gradient admits a polar decomposition  $\mathbf{F} = \mathbf{R}\mathbf{U}$  where  $\mathbf{R}$  is a rotation, and  $\mathbf{U}$  is a symmetric positive definite “stretch tensor” obeying  $\mathbf{U}^2 = \mathbf{F}^T \mathbf{F} \equiv \mathbf{C}$ .

#### 4. General finite-strain elasticity

To demonstrate the use and simplicity of the method, this paper shall focus on one broad class of materials: large-strain, 3D, purely elastic solids at constant temperature. A thermodynamically valid constitutive form for such materials is derivable with only minimal starting assumptions. Known as *hyperelasticity* theory, it has become the preeminent elasticity formulation in terms of physicality and robustness. Though other elasticity formulations exist (e.g. hypoelasticity and other stress-rate models) the next section will recall how these are in fact specific limiting approximations to hyperelasticity theory. A brief review of hyperelasticity is provided below to establish the key results and demonstrate the physical basis of the theory (see [5] for details). An analysis of more complex solid-like behaviors (e.g. elasto-plasticity, hardening, thermal elasticity) is left as future work.

In essence, one seeks a noncommittal 3D extension of 1D spring mechanics, where total relative length change determines the force in a fashion independent of deformation path. To institute this, presume that the Helmholtz free-energy per unit (undeformed) volume  $\psi$  and Cauchy stress  $\mathbf{T}$  both depend only on the local deformation:

$$\psi = \hat{\psi}(\mathbf{F}) \quad , \quad \mathbf{T} = \hat{\mathbf{T}}(\mathbf{F}) \quad (6)$$

where  $\hat{\cdot}$  is used to designate constitutive dependences on kinematic quantities. We also assume that if no deformation has occurred (i.e.  $\mathbf{F} = \mathbf{1}$ ), then  $\mathbf{T} = \mathbf{0}$ .

Some helpful physical principles refine these dependences immensely. We enforce *frame-indifference* by restricting the dependences to account for rotations. Suppose a material element is deformed by some amount, and then the deformed element is rotated. By the frame-indifference principle, the rotation should not affect the free-energy, and should only cause the stress to co-rotate. This ultimately restricts Eqs 6 to

$$\psi = \hat{\psi}(\mathbf{C}) \quad \text{and} \quad \mathbf{T} = \mathbf{R} \hat{\mathbf{T}}(\mathbf{C}) \mathbf{R}^T. \quad (7)$$

Next, we enforce *non-violation of the second law*. A continuum-level expression of the isothermal second law of thermodynamics can be written as the dissipation law

$$\rho \dot{\psi} - \mathbf{T} : \mathbf{D} \leq 0 \quad (8)$$

where  $\mathbf{D} = (\nabla \mathbf{v} + (\nabla \mathbf{v})^T)/2$  is the deformation rate, familiar from fluid mechanics. Following a procedure originally developed by Coleman and Noll [3], one can prove mathematically that Eqs 7 uphold Ineq 8 under all impossible deformations only if:

$$\mathbf{T} = 2(\det \mathbf{F})^{-1} \mathbf{F} \frac{\partial \hat{\psi}(\mathbf{C})}{\partial \mathbf{C}} \mathbf{F}^T. \quad (9)$$

Likewise,  $\mathbf{C} = \mathbf{0}$  must correspond to a local minimum of  $\psi$ . Eq 9 along with the zero deformation hypotheses compose the theory of hyperelasticity.

The above argument demonstrates how the assertions of frame-indifference and the second-law require that the assumed dependences of Eq 6 refine to the form of Eq 9. Each valid choice of  $\hat{\psi}$  gives an elasticity law that could represent a continuous elastic solid. The “deductive approach” above has become a frequently used tool in materials theory.

#### 5. Some past Eulerian attempts

To use hyperelasticity, or deductive solid modeling in general, the ability to calculate  $\mathbf{F}$  during a deformation is crucial. In Lagrangian-frame, each point is “tagged” by its start point  $\mathbf{X}$ , so  $\mathbf{F}$  can always be computed by differentiating current location against initial. In Eulerian the problem is

more subtle, as knowledge of past material locations must somehow be procured. As suggested in [11],  $\mathbf{F}$  can be directly evolved by expanding the material time derivative in Eq 5, giving

$$\mathbf{F}_t + \mathbf{v} \cdot \nabla \mathbf{F} = (\nabla \mathbf{v}) \mathbf{F}. \quad (10)$$

Unfortunately, this cannot be used to solve the general boundary value problem. The term  $\nabla \mathbf{F}$  can only be computed adjacent to boundaries if  $\mathbf{F}$  is prescribed as a boundary condition. To assign  $\mathbf{F}$  at a boundary implies that the derivative of motion in the direction orthogonal to the surface can be controlled. In the general boundary value problem, this information is outside the realm of applicability; stress tractions and displacements/velocity conditions can be applied at boundaries, but how these quantities change orthogonal to the surface arises as part of the deformation solution.

Another approach that also advects the  $\mathbf{F}$  tensor directly (more factually the tensor  $\mathbf{F}^{-1}$ ) is the Eulerian Godunov method of Miller and Colella [14]. The method solves for elastic or elasto-plastic solid deformation by treating the equations as a system of conservation laws with a nonconservative form for the advection of  $\mathbf{F}^{-1}$ . It is a sophisticated, high-order method and has had success representing solid dynamics and deformation, but is aimed primarily at unbounded domains where implementation of a boundary condition on  $\mathbf{F}$  is unneeded.

For pure elasticity, several Eulerian, rate-based approaches have been developed that avoid directly referring to  $\mathbf{F}$  but add in several approximations/assumptions. Begin by presuming isotropy. It can be shown that this reduces Eq 9 to

$$\mathbf{T} = \frac{2}{\sqrt{I_3}} \left[ I_3 \frac{\partial \hat{\psi}}{\partial I_3} \mathbf{1} + \left( \frac{\partial \hat{\psi}}{\partial I_1} + I_1 \frac{\partial \hat{\psi}}{\partial I_2} \right) \mathbf{B} - \frac{\partial \hat{\psi}}{\partial I_2} \mathbf{B}^2 \right] \quad (11)$$

where  $I_1, I_2, I_3$  are the principal invariants of the left Cauchy-Green tensor  $\mathbf{B} = \mathbf{F}\mathbf{F}^T$  [5].

One way to uphold Eq 11 involves first defining a *strain measure*  $\mathbf{E} = \mathbf{E}(\mathbf{B})$  that, among other features, must asymptote to  $\mathbf{E} = 0.5(\mathbf{F} + \mathbf{F}^T) - \mathbf{1}$  in the small displacement limit  $|\mathbf{F} - \mathbf{1}| \ll 1$ . To linear order in  $\mathbf{E}$ , the elasticity law can then be written as

$$\mathbf{T} = 2G\mathbf{E} + \lambda(\text{tr}\mathbf{E})\mathbf{1} \equiv \mathcal{C}(\mathbf{E}). \quad (12)$$

Taking the material time derivative gives  $\dot{\mathbf{T}} = \mathcal{C}(\dot{\mathbf{E}})$ . The chain rule on  $\dot{\mathbf{E}}$  generally leads to a long expression in terms of  $\mathbf{F}$  and  $\dot{\mathbf{F}}$ , which can ultimately be rewritten as some function of  $\mathbf{T}$  and  $\nabla \mathbf{v}$ .

Eulerian expansion of  $\dot{\mathbf{T}}$  introduces a term  $\mathbf{v} \cdot \nabla \mathbf{T}$ . Once again, the same problem as that encountered in Eq 10 occurs; to compute  $\nabla \mathbf{T}$ , the full Cauchy stress tensor  $\mathbf{T}$  must be assigned at the boundary. While certain components of  $\mathbf{T}$  can be controlled at a boundary—namely the traction vector  $\mathbf{T}\hat{\mathbf{n}}_{\text{bound}}$ —the components describing stresses along a plane orthogonal to the surface cannot, in general, be prescribed.

To dodge this difficulty the term  $\mathbf{v} \cdot \nabla \mathbf{T}$  is presumed to be negligible. As a consequence of neglecting stress convection, one accepts certain errors in representing dynamic phenomena. Ultimately, what remains is an Eulerian constitutive relation for the evolution of  $\mathbf{T}$

$$\mathbf{T}_t = \mathcal{C}(A(\mathbf{T}, \nabla \mathbf{v})) \quad (13)$$

where the function  $A$  derives from the choice of strain-measure. While  $\mathbf{D}$  is sometimes called the “strain-rate”, we note that it is not the time rate of change of a valid strain measure; the axes of  $\int \mathbf{D} dt$  do not rotate with the material. However,  $\dot{\mathbf{E}} \approx \mathbf{D}$  in the small displacement limit for all strain definitions. Assuming small displacement and small rate of volume change, Eq 13 reduces to a simple form known as *hypoelasticity*

$$\mathbf{T}^\circ = \mathcal{C}(\mathbf{D}) \quad (14)$$

where  $\mathbf{T}^\circ$  is an “objective stress rate” equal to  $\mathbf{T}_t$  plus extra terms that depend on the choice of strain measure.

Hypoelasticity can be seen as a specific approximation to a physically derived isotropic hyperelasticity law. Be that as it may, Eq 14 is oftentimes asserted as a starting principle by assigning

$\mathbf{T}^\circ$ , sometimes arbitrarily, from a list of commonly used stress rates— e.g. Jaumann rate, Truesdell rate, Green-Naghdi rate (see [13] for a detailed review) —thereby cutting off the connection to hyperelasticity. In fact, there are infinitely many stress rate expressions upholding frame-indifference that qualify as objective hypoelastic rates.

Rate forms for elasticity require the assumptions and approximations listed herein, which limit their applicability. The neglect of stress convection can pay heavy consequences when attempting to represent waves or other dynamic phenomena. While Eq 13 is fairly general for isotropic linearly elastic materials, the resulting equations usually require tedious calculation that must be redone if the stress/strain relation is changed. Even in the small strain limit, hypoelasticity’s presumptions of linearity and isotropy poorly represent some common materials. For instance, granular matter is nonlinear near zero strain (due to lack of tensile support), and crystalline solids are not isotropic. Rate elasticity, if used as a first principle, also offers no physical basis to account for thermodynamics, making it troublesome for theories of thermalized or non-equilibrium materials.

## 6. The reference map

To sidestep these issues, we now describe a new Eulerian approach to solid mechanics. The key is to utilize a fixed-grid field that admits a direct computation of  $\mathbf{F}$ . Define a vector field called the *reference map*  $\boldsymbol{\xi}(\mathbf{x}, t)$  by the evolution law:

$$\boldsymbol{\xi}_t + \mathbf{v} \cdot \nabla \boldsymbol{\xi} = \mathbf{0} \quad \text{for } \boldsymbol{\xi}(\mathbf{x}, t = 0) = \mathbf{x} = \mathbf{X}. \quad (15)$$

This advection law implies that  $\boldsymbol{\xi}$  never changes for a tracer moving with the flow. Combined with the initial condition, the vector  $\boldsymbol{\xi}(\mathbf{x}, t)$  indicates where the material occupying  $\mathbf{x}$  at time  $t$  originally started.

By the chain rule, a material filament obeys  $d\mathbf{X} = (\nabla \boldsymbol{\xi})d\mathbf{x}$ . Thus,

$$\mathbf{F} = (\nabla \boldsymbol{\xi})^{-1}. \quad (16)$$

Altogether, Eqs 2, 9, 15, and 16, along with the kinematic expression for the density  $\rho = \rho_0(\det \mathbf{F})^{-1}$ , compose an Eulerian system that solves exactly for hyperelastic deformation.

In essence, what we are suggesting is to obtain solid stress in a fashion similar to fluid stress. For fluids, the (shear) stress is given by  $\mathbf{D}$ , which is computed from the gradient of  $\mathbf{v}$ . Here, we advect the primitive quantity  $\boldsymbol{\xi}$  and use its gradient to construct  $\mathbf{F}$ . The stress is then obtained from  $\mathbf{F}$  by the constitutive law. This approach alleviates many of the complications discussed previously that arise when attempting to directly advect a tensorial quantity like  $\mathbf{F}$  or  $\mathbf{T}$ .

In particular, unlike the advection law of Eq 10, the reference map is easily definable on boundaries provided complete velocity/displacement boundary conditions. That is, if a boundary point originally at  $\mathbf{X}_b$  is prescribed a displacement bringing it to  $\mathbf{x}_b$  at time  $t$ , then  $\boldsymbol{\xi}(\mathbf{x}_b, t) = \mathbf{X}_b$ . We also note that  $\boldsymbol{\xi}$  is an integral quantity of  $\mathbf{F}$  and thus a smoother function. We expect this property to be of benefit numerically compared to methods that directly advect  $\mathbf{F}$  or  $\mathbf{T}$ .

The notion of a map that records initial locations of material has been defined by others in various different contexts. To these authors’ knowledge, it has never been used for the purposes of solving solid deformation as described above. Koopman *et al.* [8] use an “original coordinate” function akin to our reference map in defining a pseudo-concentration method for flow fronts. The inverse of  $\boldsymbol{\chi}$  at time  $t$ , which is indeed equivalent to the  $\boldsymbol{\xi}$  field, is also discussed in Belytschko [2] for use in finite element analysis.

## 7. Implementation

In this section, we describe the discretization of the above system of equations. Our general strategy is to first evaluate  $\mathbf{T}$ , then update  $\mathbf{v}$  using Eq 2, and finally evolve  $\boldsymbol{\xi}$  with 15. Time derivatives in Eqs 2, and 15 are discretized as a simple Euler step,

$$\partial_t \boldsymbol{\xi}(\mathbf{x}, t) = (\boldsymbol{\xi}(\mathbf{x}, t + \Delta t) - \boldsymbol{\xi}(\mathbf{x}, t)) / \Delta t.$$

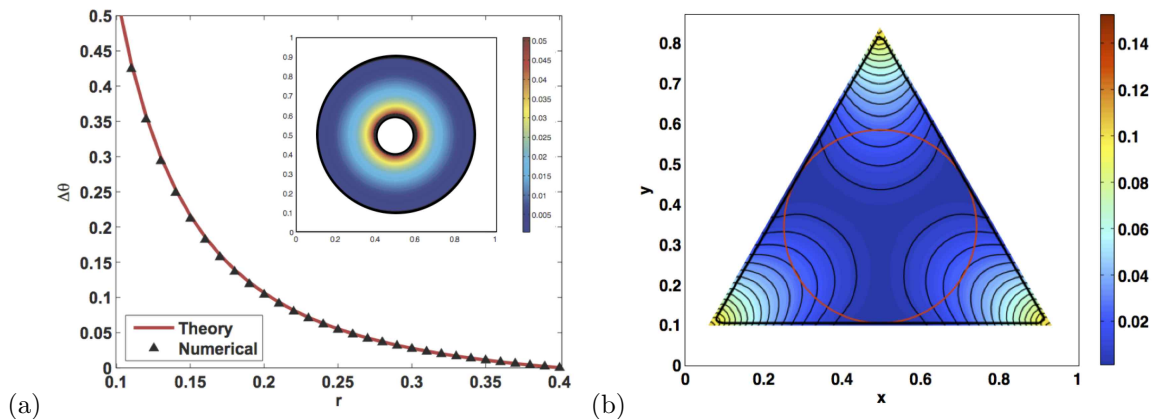


Figure 1: (a) Angular displacement of washer after inner wall rotation. Inset displays the scalar displacement field; note high radial symmetry though the scheme uses a fixed *cartesian* grid. (b) Displacement field as a function of final location after an elastic disk (red outline) is stretched into a triangle. Both tests were performed on a 100x100 grid.

On a two-dimensional grid, with grid spacing  $h$ , the velocity  $\mathbf{v}$  and reference map  $\boldsymbol{\xi}$  are located at corner points  $(i, j)$ , while stresses  $\mathbf{T}$  are located at cell centers,  $(i + \frac{1}{2}, j + \frac{1}{2})$ . Thus, away from any boundary, we can compute by finite difference  $\partial_x \boldsymbol{\xi}$  at the mid-point of horizontal grid edges, and similarly,  $\partial_y \boldsymbol{\xi}$  on vertical grid edges,

$$\partial_x \boldsymbol{\xi}_{(i+\frac{1}{2}, j)} = \left( \boldsymbol{\xi}_{(i+1, j)} - \boldsymbol{\xi}_{(i, j)} \right) / h. \quad (17)$$

We obtain  $\nabla \boldsymbol{\xi}$  at cell centers by averaging, allowing us to compute the deformation gradient tensor  $\mathbf{F}$  using Eq 16, and thus  $\mathbf{B}$ . We now can define stresses at cell centers by specifying the hyperelasticity law. We compute  $\partial_x \mathbf{T}$  at the mid-point of vertical grid edges, and similarly,  $\partial_y \mathbf{T}$  on horizontal grid edges,

$$\partial_x \mathbf{T}_{(i, j+\frac{1}{2})} = \left( \mathbf{T}_{(i+\frac{1}{2}, j+\frac{1}{2})} - \mathbf{T}_{(i-\frac{1}{2}, j+\frac{1}{2})} \right) / h.$$

As a result, we obtain  $\nabla \cdot \mathbf{T}$  at cell corners, where  $\mathbf{v}$  is stored. Finally,  $\nabla \mathbf{v}$  in equation 2, can be discretized in the same manner as  $\nabla \boldsymbol{\xi}$ . Additionally, since Eq 15 is an advection equation, we use a WENO discretization for  $\nabla \boldsymbol{\xi}$  to guarantee stability [12].

In order to solve the system with irregular boundaries, we introduce a level set function,  $\phi(x)$ . We define  $\phi(x) > 0$  inside the solid,  $\phi(x) \leq 0$  outside, thus implicitly representing the domain boundary as the zero level set of  $\phi(x)$ . Choosing  $\phi(x)$  to be a signed distance function, i.e.  $\|\nabla \phi(x)\| = 1$ , allows us to compute the cut-cell length  $\alpha$ , with  $0 \leq \alpha \leq 1$ . For example, if the boundary cuts a horizontal cell edge, i.e.  $\phi_{left} \cdot \phi_{right} \leq 0$ , then  $\alpha = \frac{|\phi_{left}|}{|\phi_{left}| + |\phi_{right}|}$ . Here, we must change the discrete derivatives in Eq 17. Assuming that  $\phi_{left} = \phi_{(i, j)} > 0$ ,

$$\partial_x \boldsymbol{\xi}_{(i+\frac{1}{2}, j)} = \left( \boldsymbol{\xi}_{right} - \boldsymbol{\xi}_{(i, j)} \right) / \alpha h$$

where  $\boldsymbol{\xi}_{right}$  is a boundary condition for  $\boldsymbol{\xi}$ . Other derivatives near boundaries are treated in the same manner.

## 8. Results

### 8.1. Static solutions

In this section we present two large-deformation numerical tests, both in plane-strain for simplicity. To rigorously test the method, each case models a non-trivial, inhomogeneous deformation.

First, we solve our system in a circular washer geometry for which the outer wall is fixed and the inner wall is rotated over a large angle. Under the Levinson-Burgess hyperelasticity law (see below), this environment has an analytical solution, which we use to verify the consistency/correctness of the method. Second, we solve the deformation of a disk being stretched into a triangular shape, also utilizing the Levinson-Burgess law. This has no analytical solution, and demonstrates the method's applicability in cases where the reference and deformed boundary sets differ. We focus here on static solutions, obtained by enforcing the boundary conditions and waiting for transients to pass. Artificial viscosity was added to the stress law to expedite collapse to the static solution.

The Levinson-Burgess free-energy function, after application of Eq 11, induces the following stress law under plane-strain conditions [6]

$$\mathbf{T} = f_1(I_3) \mathbf{B} + f_2(I_1, I_3) \mathbf{1} \quad (18)$$

where  $I_1 = \text{tr}\mathbf{B}$ ,  $I_3 = \det\mathbf{B}$  are invariants of the  $\mathbf{B}$  tensor, with  $f_1(I_3) = G(3 + 1/I_3)/(4\sqrt{I_3})$  and  $f_2(I_1, I_3) = G\sqrt{I_3}(\kappa/G - 1/6 + (1 - I_1)/(4I_3^2)) - G/3 - \kappa$ . In the unstrained state,  $\kappa$  and  $G$  represent the bulk and shear moduli. Throughout, we use  $\kappa = G = 100$  kPa.

*Circular washer shear.* The analytical static displacement field is  $\Delta\theta = A - B/r^2$  and  $\Delta r = 0$  where,  $A$  and  $B$  are constants that fit the boundary conditions  $\Delta\theta_{in} = \pi/6$  and  $\Delta\theta_{out} = 0$ . The graph in Figure 1(a) shows excellent agreement between our numerical solution (sampled along the central horizontal cross-section) and the analytical. We have observed equally high agreement levels when the inner wall rotation angle is varied.

*Stretched Disk.* The unstressed material shape is a disk that is inscribed perfectly within its final equilateral triangular shape. For  $\mathbf{x}_b$  on the triangle edge, the boundary condition for the final deformed body is  $\boldsymbol{\xi}(\mathbf{x}_b) = \frac{r_0\mathbf{x}_b + d(\mathbf{x}_b)\mathbf{x}_{cen}}{r_0 + d(\mathbf{x}_b)}$  where  $\mathbf{x}_{cen}$  is the disk center,  $r_0$  the disk radius, and  $d(\mathbf{x}_b)$  the distance between the disk edge and the triangle as measured along the radial segment containing  $\mathbf{x}_b$ . Hence, each point on the disk edge is moved outward radially to the triangle. The final, static displacement field is shown in figure 1(b).

## 8.2. Dynamic solutions

In this section, we display the method's ability to accurately track the motion of a large-strain compression wave. Recall from section 5, that dynamic correctness is sacrificed in many stress-rate models by neglecting stress convection terms. The reference map on the other hand, enables high-accuracy representation of elasto-dynamics as shall now be demonstrated.

In order to check for the ability of the method to handle dynamic situations, we choose to produce an analytical solution for an elastic compression wave. For this purpose, consider a material obeying the following large-strain elasticity law,

$$\mathbf{T} = \kappa(\mathbf{V} - \mathbf{1})$$

for  $\mathbf{V} \equiv \sqrt{\mathbf{B}}$  the left stretch tensor. The material body is a rectangular slab constrained in the thickness direction (i.e. plane-strain conditions). The unstressed material density is uniform and has a value  $\rho_0$ .

Under this constitutive law, the following  $\boldsymbol{\xi}$  and  $\mathbf{v}$  fields give an exact, analytical solution for a rightward moving compression wave passing through the slab:

$$\hat{\mathbf{x}} \cdot \boldsymbol{\xi}(x, y, t) = x + \frac{1}{2}\text{Erf}(x - ct) \quad (19)$$

$$\hat{\mathbf{x}} \cdot \mathbf{v}(x, y, t) = c \left( 1 - \frac{1}{1 + \frac{1}{\sqrt{\pi}}e^{-(x-ct)^2}} \right). \quad (20)$$

Due to symmetry, the  $\hat{\mathbf{y}}$  and  $\hat{\mathbf{z}}$  components of both fields do not change from their initial, unstressed values. The constant  $c = \sqrt{\kappa/\rho_0}$  is the wave speed. This solution invokes a large-strain deformation

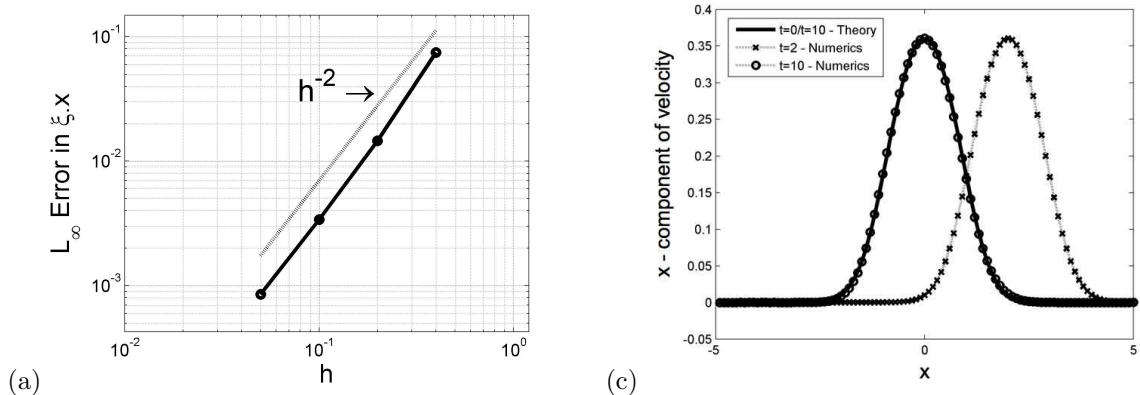


Figure 2: (a) Global convergence of the  $L_\infty$  norm of the error in  $\xi$  (connected dots). We observe a second order rate of convergence. (b) Travelling  $\hat{\mathbf{x}} \cdot \mathbf{v}$  wave through one full period  $t = [0, 10]$ . Comparison between analytical and numerical solutions.

with compressive strain as high as  $|\hat{\mathbf{x}} \cdot (\mathbf{V} - \mathbf{1})\hat{\mathbf{x}}| \approx 36\%$  at the center of the pulse. Consequently, this represents a realistic test of the ability of the present approach to tackle dynamic effects as well as large-strain deformation.

The equations are discretized in space as before, but for the time discretization we embed the Euler step described above into a standard second order Runge-Kutta scheme [15]. The stability restriction of this fully explicit scheme is so that  $\Delta t < \alpha \min(\Delta x, \Delta y) \sqrt{\kappa/\rho_0}$ , for some small constant  $\alpha$ . From this approach we expect second order global convergence.

In order to verify the convergence rate, we set up a two-dimensional doubly-periodic domain  $\Omega = [-5, 5] \times [-5, 5]$ . We use Eqs 19 and 20 at  $t = 0$  as the initial condition, with  $c = \kappa = \rho_0 = 1$ . The travelling wave solution should come back to its original shape and location at  $t = 10$ . For a sequence of grids with  $h = \Delta x = \Delta y = \{\frac{2}{40}, \frac{2}{20}, \frac{2}{10}, \frac{2}{5}\}$ , we set  $\Delta t$  using  $\alpha = \frac{1}{10}$ , and compute the  $L_\infty$  error of  $\xi$ ,  $E_\infty^\xi(h)$  as,

$$E_\infty^\xi(h) = \sup_{\{x,y\} \in \Omega} |\hat{\mathbf{x}} \cdot \xi(x, y, t = 10) - \hat{\mathbf{x}} \cdot \xi(x, y, t = 0)|.$$

We report in Figure 2(a) the expected second order global convergence. The convergence rate between the two finest grids,  $h = \frac{2}{10}$  and  $h = \frac{2}{5}$ , is computed to be 1.97. We have also found nearly identical convergence properties for the velocity; the  $x$  velocity's convergence rate is found to be 1.99 between the two finest grids. We conclude the scheme is globally second order accurate for all dynamic variables, confirming its ability to capture dynamic solutions under large-strain elasticity.

Finally, Figure 2(b) shows one-dimensional cross sections for  $\hat{\mathbf{x}} \cdot \mathbf{v}$  at different times. The solid line represents the exact solution computed from Eq 20 at  $t = 0$ , which, by periodicity of the domain, also corresponds to the solution at  $t = 10$ . We see that the exact solution and numerical solution agree well for  $h = \frac{2}{10}$ , a rather coarse grid. We also plot the numerical solution at  $t = 2$  for illustrative purposes.

## 9. Conclusion and future work

This work has demonstrated the validity of the reference map for use in reformulating and simulating solid deformation under a completely Eulerian framework. There are still several avenues of future investigation. Other material models are to be simulated, most notably elasto-plastic laws with and without rate-sensitivity. Also, the reference map has potential to simplify the simulation of fluid/solid interactions, due to both phases having a similar Eulerian treatment. Our preliminary results on this front are promising, and shall be reported in a future paper. Also, a method to



institute traction boundary conditions within this framework, especially the traction-free condition, would be important future study. This may ultimately be accomplished with a fluid/solid framework, by treating traction-free boundaries as surfaces of interaction with a pressure-free, stationary fluid.

## Acknowledgements

K. Kamrin would like to acknowledge support from the NDSEG and NSF GRFP fellowship programs. J.-C. Nave would like to acknowledge partial support by the National Science Foundation under grant DMS-0813648.

## References

- [1] L. Anand and C. Su. A theory for amorphous viscoplastic materials undergoing finite deformations, with application to metallic glasses. *J. Mech. Phys. Solids*, 53:1362–1396, 2005.
- [2] T. Belytschko, W. K. Liu, and B. Moran. *Nonlinear Finite Elements for Continua and Structures*. J. Wiley and Sons, 2000.
- [3] B. D. Coleman and W. Noll. The thermodynamics of elastic materials with heat conduction and viscosity. *Arch. Ration. Mech. Anal.*, 13:167–178, 1963.
- [4] M. L. Falk and J. S. Langer. Dynamics of viscoplastic deformation in amorphous solids. *Phys. Rev. E*, 57:7192–7205, 1998.
- [5] M. E. Gurtin. *An Introduction to Continuum Mechanics*. Academic Press, 1981.
- [6] D. M. Haughton. *Q. Jl Mech. appl. Math.*, 46:471–486, 1993.
- [7] A. Hoger. The material time derivative of logarithmic strain. *Int. J. Solids Structures*, 22:1019–1032.
- [8] A. J. Koopman, H. J. M. Geiselaers, K. E. Nilsen, and P. T. G. Koenis. Numerical flow front tracking for aluminium extrusion of a tube and a comparison with experiments. *Int. J. Mater. Form.*, Suppl 1:423–426, 2008.
- [9] E. H. Lee. Elastic plastic deformation at finite strain. *J. Appl. Mech.*, 36:1–6, 1969.
- [10] A. Lemaître. Rearrangements and dilatency for sheared dense materials. *Phys. Rev. Lett.*, 89:195503, 2002.
- [11] C. Liu and N. J. Walkington. An eulerian description of fluids containing visco-elastic particles. *Arch. Rational Mech. Anal.*, 159:229–252, 2001.
- [12] X.-D. Liu, S. Osher, and T. Chan. Weighted essentially non-oscillatory schemes. *J. Comput. Phys.*, 115:200–212, 1994.
- [13] A. Meyers, H. Xiao, and O. T. Bruhns. Choice of objective rate in single parameter hypoelastic deformation cycles. *Comput. Struct.*, pages 1134–1140, 2006.
- [14] G. H. Miller and P. Colella. A high-order eulerian godunov method for elasticplastic flow in solids. *J. Comput. Phys.*, 167:131–176, 2001.
- [15] C.-W. Shu and S. Osher. Efficient implementation of essentially non-oscillatory shock-capturing schemes. *J. Comput. Phys.*, 77:439–471, 1988.